

Model-Free Rheo-AFM Probes the Viscoelasticity of Tunable DNA Soft Colloids

José A. Moreno-Guerra, Ivany C. Romero-Sánchez, Alejandro Martínez-Borquez, Manlio Tassieri, Emmanuel Stiakakis, and Marco Laurati*

Atomic force microscopy rheological measurements (Rheo-AFM) of the linear viscoelastic properties of single, charged colloids having a star-like architecture with a hard core and an extended, deformable double-stranded DNA (dsDNA) corona dispersed in aqueous saline solutions are reported. This is achieved by analyzing indentation and relaxation experiments performed on individual colloidal particles by means of a novel model-free Fourier transform method that allows a direct evaluation of the frequency-dependent linear viscoelastic moduli of the system under investigation. The method provides results that are consistent with those obtained via a conventional fitting procedure of the force-relaxation curves based on a modified Maxwell model. The outcomes show a pronounced softening of the dsDNA colloids, which is described by an exponential decay of both the Young's and the storage modulus as a function of the salt concentration within the dispersing medium. The strong softening is related to a critical reduction of the size of the dsDNA corona, down to $\approx 70\%$ of its size in a salt-free solution. This can be correlated to significant topological changes of the dense star-like polyelectrolyte forming the corona, which are induced by variations in the density profile of the counterions. Similarly, a significant reduction of the stiffness is obtained by increasing the length of the dsDNA chains, which we attribute to a reduction of the DNA density in the outer region of the corona.

1. Introduction

Several materials of daily use are made of colloidal particles dispersed in a continuous medium, including among many others paints, cosmetics, foodstuff, fluids for oil extraction, and ferrofluids.^[1] Of great importance for many applications is the knowledge of their state diagram, i.e., whether they exist in a gas, fluid, or solid state.^[1,2] This is mainly governed by the interactions between the colloidal particles that can be of different *nature* and coexist at the same time, and include for instance van der Waals, electrostatic, steric, and magnetic forces.^[1,3] The relative contribution of these forces depend on several factors, such as the constituent materials of the colloids, their shape, internal architecture, and surface properties.^[4] Moreover, recently it has been proposed that the degree of softness, or compressibility, of the colloidal particles influences substantially their bulk phase behavior.^[5,6] In particular, it has been shown that the transition point from a fluid to a solid crystalline state occurs at growingly larger packing fractions for increasing


softer particles; with a fluid-solid coexistence state that progressively disappears.^[6] The softness of the colloidal particles also governs the formation of crystalline states such as exotic lattices like σ , A15, and simple hexagonal,^[7–10] which are usually not observed in the case of hard colloidal spheres. Furthermore, the formation of nonequilibrium solids such as glasses and jams also shifts to higher packing fraction values.^[5,6] In addition, in charged systems such as ionic microgels, the softness is affected by the complex interplay between packing and counterions' distribution, so that significant deswelling can be observed at large packing fractions due to the osmotic pressure generated by the expelled counterions.^[11,12]

Over the past few years, several experimental techniques have been proposed for measuring the particles' softness; these include centrifugation,^[13,14] micropipette aspiration,^[15,16] dynamic light scattering combined with variations of the osmotic pressure,^[17] microdrop confinement,^[18] microfluidic flow,^[19] and atomic force microscopy (AFM).^[20–22] Interestingly, all these methods provide a measure of the "elasticity" of the particles by means of their bulk or Young's modulus. However, it must be noted that in most cases colloids are made of materials like polymers, biopolymers, or gels,

J. A. Moreno-Guerra, I. C. Romero-Sánchez, Dr. A. Martínez-Borquez, Dr. M. Laurati
División de Ciencias e Ingenierías
Universidad de Guanajuato
Lomas del Bosque 103, 37150 León, Mexico
E-mail: mlaurati@fisica.ugto.mx

Dr. M. Tassieri
Division of Biomedical Engineering
School of Engineering
University of Glasgow
Glasgow G12 8LT, UK

Dr. E. Stiakakis
Forschungszentrum Jülich
Institute of Complex Systems 3
Leo-Brandt-Strasse, 52425 Jülich, Germany

 The ORCID identification number(s) for the author(s) of this article can be found under <https://doi.org/10.1002/smll.201904136>.

© 2019 The Authors. Published by WILEY-VCH Verlag GmbH & Co. KGaA, Weinheim. This is an open access article under the terms of the Creative Commons Attribution License, which permits use, distribution and reproduction in any medium, provided the original work is properly cited.

DOI: 10.1002/smll.201904136

which have an inherent *viscoelastic nature*. This indeed plays an important role in systems with dense particle packings (e.g., crystals, glasses, and jams) by affecting their dynamics and structural relaxations, and its importance has been already recognized for biological tissues^[23] and cells, especially under pathological conditions.^[24,25] Most of these studies have been performed by using time-dependent AFM indentation measurements, also known as “indentation-relaxation” experiments. In these cases, the materials’ viscoelastic properties are usually obtained by modeling the force relaxation curve with either a generalized Maxwell model^[24] or more complex fractional models,^[26] from which parametric quantities such as the bulk modulus and the effective viscosity are educed. An alternative, but time-consuming and limited in the range of explored frequencies, AFM method is based on the measurement of the frequency-dependent amplitudes and phase-shift between an imposed oscillatory indentation and the relative force response of the material detected via the cantilever deflection.^[27–31] In this work we exploit a novel and simple broadband method,^[25] in which the time-dependent force relaxation curve is Fourier transformed to obtain the frequency-dependent linear viscoelastic properties of the system under investigation without the adoption of any viscoelastic model to interpret the data, as described below.

Amongst a great variety of available soft colloids, star-like double-stranded DNA (dsDNA) colloids have been recently introduced as a novel class of polyelectrolyte grafted colloids.^[32] Indeed, in contrast to solid charged colloids, the complex architecture of their corona allows to accommodate a large number of counterions that provide unique properties. For instance, under salt-free conditions and for relatively large grafting densities the corona incorporates all counterions, which induce an osmotic swelling and a rod-like conformation of the arms (i.e., they are completely stretched). In particular, the DNA stretching, while costing in terms of entropy, maximizes the available space for the mobile counterions, overall resulting in an increase of entropy. This configuration leads to an osmotic imbalance between the interior of the corona and the bulk. With the addition of NaCl the osmotic imbalance is progressively reduced until balance is reached and the corona deswells and shrinks, with a salt-dependent size in agreement with a modified blob model for dense polyelectrolyte brushes.^[32,33] Moreover, star-like dsDNA colloids show interesting behavior in overcrowded conditions, where for example the formation of crystalline states through particle faceting without corona interpenetration has been observed in salt-free dispersions; a process that is novel for hairy colloids, but often observed in microgels.^[12,34] Interpenetration of the dsDNA coronas occurs instead with the addition of salt. Despite these interesting phenomena, a relationship between the mechanical properties of a single hairy colloid and either the salt-induced changes of its corona conformation or their phase behavior is *still missing* from the literature.

In this work we address this lack of knowledge by exploiting the effectiveness of a novel Rheo-AFM technique. In particular, we measure the *yet unexplored* viscoelastic properties of single dsDNA star-like colloids as function of salt concentration, size, number, and length of the grafted DNA chains. Notably, all these properties are rationally tunable and can be effectively characterized by means of Rheo-AFM measurements. The data are analyzed by using two complementary approaches: I) by modeling the force relaxation-curves with a modified fractional Hertz model

and II) by Fourier transforming the same curves by means of a novel method recently proposed by Tassieri and co-workers.^[25] We investigate the viscoelastic *nature* of single-colloidal particles as a function of salt concentration and dsDNA chain length for a fixed number of grafted DNA chains (functionality $f = 2 \times 10^5$ chains per particle). For the arm length and the f values investigated here, the DNA coated colloids behave as osmotic stars under salt-free conditions, i.e., the size of the dsDNA corona equals the contour length of the grafted chains.^[35]

We anticipate that our records reveal a pronounced softening of the dsDNA corona with increasing of salt concentration. This can be mainly attributed to the conformational changes of the polyelectrolyte corona, with an abrupt softening at a critical size of the DNA corona (or salt concentration). Moreover, we observe a similar softening of the particles when the DNA chain length is increased (i.e., doubled) and we attribute this to the reduced chain density in the outer layer of the corona. Finally, we shall highlight that the results reported in this manuscript are of particular interest to all those studies aimed at gaining a better understanding of the mechanical properties of a broad range of soft colloidal particles, such as polyelectrolyte brushes and microgels^[36–40] and microgel particles.^[5,16,17]

2. Results and Discussion

2.1. Indentation and Relaxation Experiments

Figure 1 shows a schematic representation of the AFM setup adopted to perform indentation and relaxation experiments. A colloidal AFM tip was used to indent a single colloidal particle attached to a glass substrate and dispersed in an open liquid cell environment (see the Experimental Section for more details). By following the experimental procedure introduced by Tassieri and co-workers,^[25] the measurement protocol consisted of the following steps: I) the colloidal probe was equilibrated above the sample surface for 5 s; II) the probe was successively indented into the sample to a predefined indentation depth $\delta_0 < 10\%$ of the sample thickness, i.e., the particle diameter; III) the probe was maintained at constant height within the sample; IV) the probe was retracted from the sample. The contact point

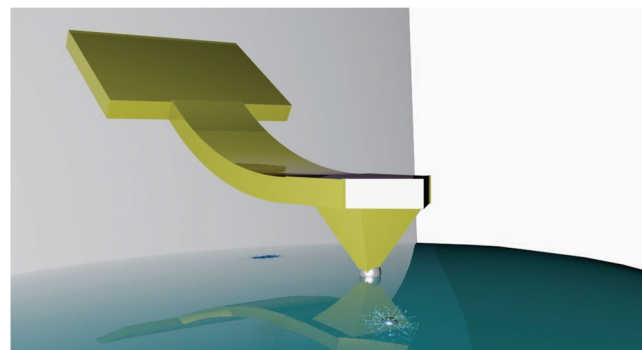


Figure 1. A schematic representation of the experimental setup. A spherical tip of an AFM cantilever is brought into contact with a dsDNA star-like colloid suspended in water within an open liquid cell environment. The colloid is attached to a glass substrate.

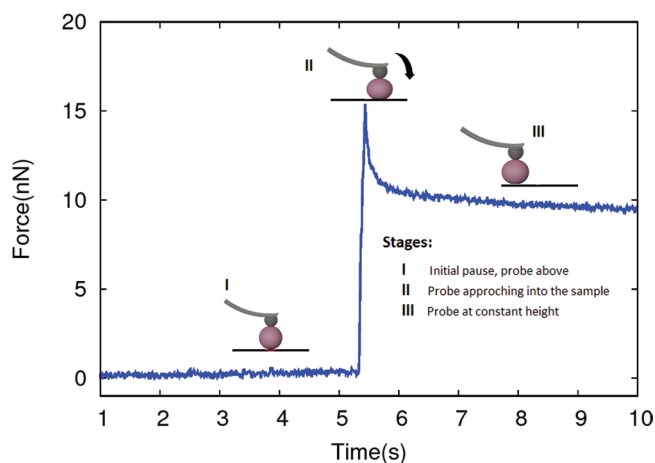


Figure 2. Force versus time curve of a typical indentation and relaxation experiment, which consists of three sequential steps as shown in the figure: I) probe equilibration; II) probe approach and indentation; III) probe at constant depth into the sample.

between the probe and the colloidal particle was previously determined from a force–distance curve. The force versus time curve corresponding to steps (I to III) of a typical experiment is shown in **Figure 2**. During step (I), in which the tip lies above the sample, the registered force is zero. When the tip starts to indent the sample (step II), the force rapidly increases, reaching a maximum value at the deepest indentation point; then the force starts to relax, potentially revealing the viscoelastic properties of the material (step III).

Due to the small applied indentation depth, the regime of deformation can be described by means of a modified version of the Hertz model for a spherical indenter.^[41,42] The relaxation of the force during step (III) was sampled at a frequency of 100 Hz. This is the upper frequency limit of the Piezo stage (controlling the cantilever height), above which it moves out from its linear operational regime. The probe approaching speed was chosen to be equal to 20 $\mu\text{m/s}$ in all the experiments. At this loading rate no overshoot of the loading force^[43] were observed; corroborating the adoption of the Hertz model.

Measurements were performed on dsDNA hairy colloids suspended in water solutions at seven different concentrations of NaCl, i.e., $c_s = 0.0, 0.005, 0.025, 0.050, 0.100, 0.250, 1.000$ M. The synthesis of the colloidal particles follows the protocol introduced in a previous work^[32] and here reported in the experimental section for the convenience of the reader. The experiments were performed on colloidal particles having a streptavidin-coated polystyrene sphere of radius $R_{ps} = 0.49$ μm as core, on the surface of which biotin terminated dsDNA chains were grafted. The dsDNA chain length was equal to 10 kbp, which corresponds to a contour length of $L_c \approx 3.4$ μm in salt-free water.^[32] The functionality $f = 2 \times 10^5$ chains per particle. In addition, as a means of comparison, dsDNA hairy colloids with 20 kbp chain length having the same functionality f and core radius of those described above, were tested to investigate the effect of chain length on particle softness. Note that due to the osmotic nature of the corona, for 20 kbp chain

length the size of the corona is double the size for 10 kbp, i.e., $L_c \approx 7.8$ μm in salt-free water.

2.2. Force Relaxation Curves: Elastic and Viscous Contributions

In the case of a relatively small indentation of a viscoelastic sphere of radius R_2 by means of a (solid) spherical tip of radius R_1 (which is to a first approximation a good representation of our system), the time-dependent force relaxation can be written as^[44,45]

$$F(t) = \frac{8}{3(1-\nu)} \left[\left(\frac{1}{R^*} \right)^{1/3} + \left(\frac{1}{R_2} \right)^{1/3} \right]^{-3/2} \int_{-\infty}^t G(t-\tau) \frac{d\delta^{3/2}(\tau)}{d\tau} d\tau \quad (1)$$

where $1/R^* = 1/R_1 + 1/R_2$, ν is the Poisson's ratio, $G(t)$ and $\delta(t)$ are the time-dependent relaxation modulus and indentation depth, respectively. Notably, in the limit of $R_2 \rightarrow \infty$, which corresponds to the indentation of a flat surface by means of a spherical tip, the pre-factor in Equation (1) only depends on R_1 and ν , returning the well-known expression of the Hertz model. In the specific case of a finite step-indentation, for which the time derivative of $\delta(t)$ is equal to zero before and after the time interval required to perform the indentation of amplitude δ_0 (step II, in Figure 2), Equation (1) simplifies as it follows (please see the Supporting Information for an extended derivation)

$$F(t) = \frac{8\delta_0^{3/2}}{3(1-\nu)} \left[\left(\frac{1}{R^*} \right)^{1/3} + \left(\frac{1}{R_2} \right)^{1/3} \right]^{-3/2} G(t) \quad (2)$$

Therefore, the time-dependent relaxation modulus $G(t)$ of the viscoelastic colloid is simply proportional to the measured force and ready to be modeled.^[24,26,46] Notably, once the experimental conditions have been defined, the constant of proportionality between $F(t)$ and $G(t)$ in Equation (2) is fully determined. In this work the parameters are $R_1 = 4$ μm , $\delta_0 = 0.1\text{--}0.4$ μm , depending on sample, and $\nu = 0.5$ according to the values reported in the literature.^[47] Notice that, small variations of ν would only shift the magnitude of the outcomes, but not their frequency behavior. In order to calculate the radius of the colloids as a function of c_s , we have used the following relation: $R_2 = R_{ps} + L$. Where $R_{ps} = 0.49$ μm is the radius of the polystyrene inner core, which is independent by c_s , and $L(c_s)$ is the size of the dsDNA corona. The latter has been determined by using the following scaling law presented by others in a previous work,^[32] $L \approx c_s^{-0.11}$.

The simplest analytical expression for describing the temporal behavior of $G(t)$ is a single mode Maxwell model, which is a single exponential decay with a characteristic relaxation time^[48] determined by the relative contribution of the elastic (G_0) and the viscous (η_0) components of the model; i.e., $G(t) = G_0 \exp(-t/\tau)$, with $\tau = \eta_0/G_0$. However, it must be noted that, none of our measurements would have been adequately modeled by means of this simple expression, which implies that i) the force fully decays to zero at long times ii) via a single

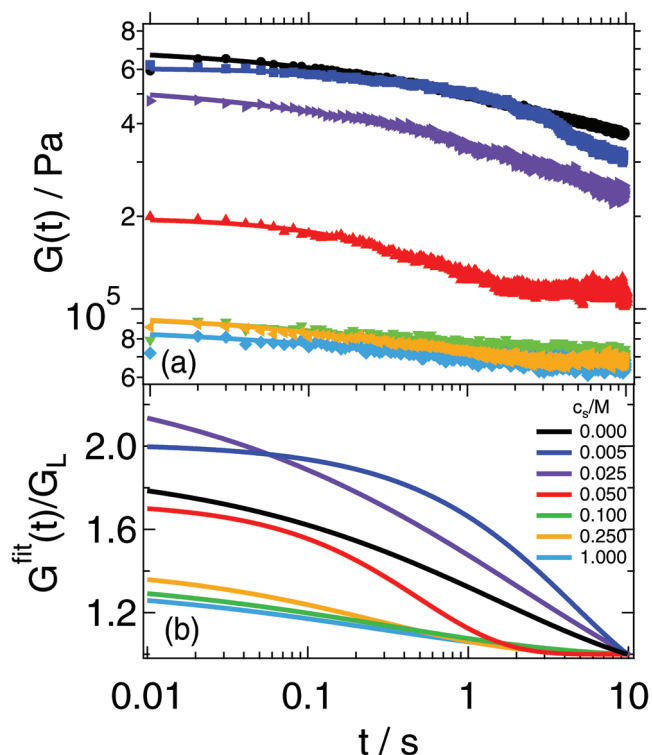


Figure 3. a) Shear relaxation modulus ($G(t)$) versus time for dsDNA hairy colloids dispersed in water at different concentrations of salt c_s : 0 M (●), 0.005 M (■), 0.025 M (▴), 0.05 M (▲), 0.1 M (▼), 0.25 M (◀), and 1 M (◆). Lines are the data best fits of Equation (3). b) The best-fit curves as in (a), but normalized by their value at the longest measured time, G_L .

relaxation process, which is not the case of our experiments as we shall demonstrate below. Therefore, in order to account for the existence of a residual (rubber-like) modulus G_R and a distribution of relaxation times,^[26] we have adopted the following stretched exponential expression of $G(t)$:

$$G(t) = G_R + G_0 \exp[-(t/\tau)^\beta] \quad (3)$$

with an average relaxation time determined as $\langle \tau \rangle = (\eta_0/G_0)^{1/\beta}$. The best fits of the experimental data of Equation (3) are shown in Figure 3 and the output parameters G_0 , G_R , η_0 , and β are reported in Table 1 together with the relative errors, which correspond to one standard deviation, as obtained from the fits.

Table 1. Fitting parameters and relative errors obtained by interpreting the force relaxation data in Figure 3 via Equation (3). Errors correspond to one standard deviation obtained from the fits.

c_s [M]	G_0 [10^5 Pa]	G_R [10^5 Pa]	η_0 [10^5 Pa s]	β
0	3.86 ± 0.07	3.29 ± 0.03	5.9 ± 0.1	0.41 ± 0.01
0.005	3.71 ± 0.03	2.35 ± 0.03	17.1 ± 0.4	0.72 ± 0.01
0.025	3.9 ± 0.2	1.62 ± 0.1	8.4 ± 0.05	0.35 ± 0.02
0.05	0.84 ± 0.02	1.14 ± 0.01	0.41 ± 0.01	0.81 ± 0.03
0.10	0.28 ± 0.05	0.70 ± 0.005	0.09 ± 0.02	0.37 ± 0.06
0.25	0.29 ± 0.01	0.68 ± 0.004	0.08 ± 0.005	0.51 ± 0.01
1.00	0.23 ± 0.04	0.65 ± 0.005	0.06 ± 0.015	0.39 ± 0.06

Figure 3 shows the shear relaxation modulus curves (i.e., the force relaxation ($F(t)$) via Equation (2)) obtained from the indentation measurements on the dsDNA hairy colloids suspended in water at different salt concentrations c_s . The absolute value of $G(t)$ decreases with increasing c_s , implying that a smaller force is required to reach the same relative indentation depth $\delta_0 \approx 5\%$ and therefore inferring a softening of the dsDNA particle's corona with increasing the salt content in the solution. For most of the measurements the decay of the shear relaxation modulus with time is evident as well as the existence of a finite plateau value. Moreover, it can be seen that the addition of salt to the solution (i.e., at $c_s = 0.005$ M) induces first a slow-down of the relaxation process (when compared with the salt-free case) and then a faster decay for larger values of c_s . This is highlighted in Figure 3b, where we report the best fits of the experimental data by means of Equation (3), but normalized by their values at long times (i.e., G_R).

In Figures 4 and 5 are reported the parameter values of the best fits of Equation (3) as a function of salt concentration c_s . From these diagrams it can be seen that both the total modulus $G_T = G_0 + G_R$ and the residual modulus G_R show a reduction with increasing of c_s (Figure 4a, which indicates a progressive softening of the colloidal particles). Notice that the presence of a residual modulus indicates a kind of glassy behavior of the corona. Interestingly, the salt concentration dependence of both G_T and G_R can be described with an exponential decay having the following expression: $G_i = G_i^0 \exp(-c_s/c_s^0) + B$; where $i = T, R$ and B is a baseline value. We find that for both the moduli $c_s^0 \approx 0.026$ M. Figure 4b shows the values of G_T plotted against the salt-dependent corona thickness L relative to its value in the absence of salt, L_0 . It can be seen that the particle stiffness (i.e., G_T) shows a sharp transition by almost an order of magnitude at $L/L_0 \approx 0.72$ (which corresponds to a salt concentration of $c_s = 0.025$ M) between the two well-defined regimes, within which only a moderate reduction of the modulus is observed as a function of L (or equivalently of c_s). This is a riveting finding that suggests the existence of a critical size of the corona, below which a significant softening of the colloidal particles is observed. This critical size of the corona corresponds to the end of the osmotic regime. The inset of Figure 5 shows the ratio G_R/G_T , which reveals an initial decrease at salt concentration values of $c_s = 0.005$ and 0.25 M, followed by an increase at $c_s = 0.05$ and 0.1 M, and then the ratio remains almost constant for $c_s = 0.25$ and 1 M. Given that for viscoelastic fluids G_R should tend to 0, an increase of the ratio G_R/G_T indicates a tendency of the system to behave

like a viscoelastic solid (e.g., gels and rubbers). Therefore, the initial reduction of G_R/G_T can be seen as a transition to a more fluid behavior of the corona, followed by a transition to a behavior closer to a viscoelastic solid; however, with a continuously decreasing modulus as shown by the monotonic decrease of G_T . The inset of Figure 4 shows the salt concentration functionality of the model viscosity η_0 , which exhibits an initial increase followed by a pronounced decrease of almost two orders of magnitude. A similar behavior is observed for the characteristic average relaxation time

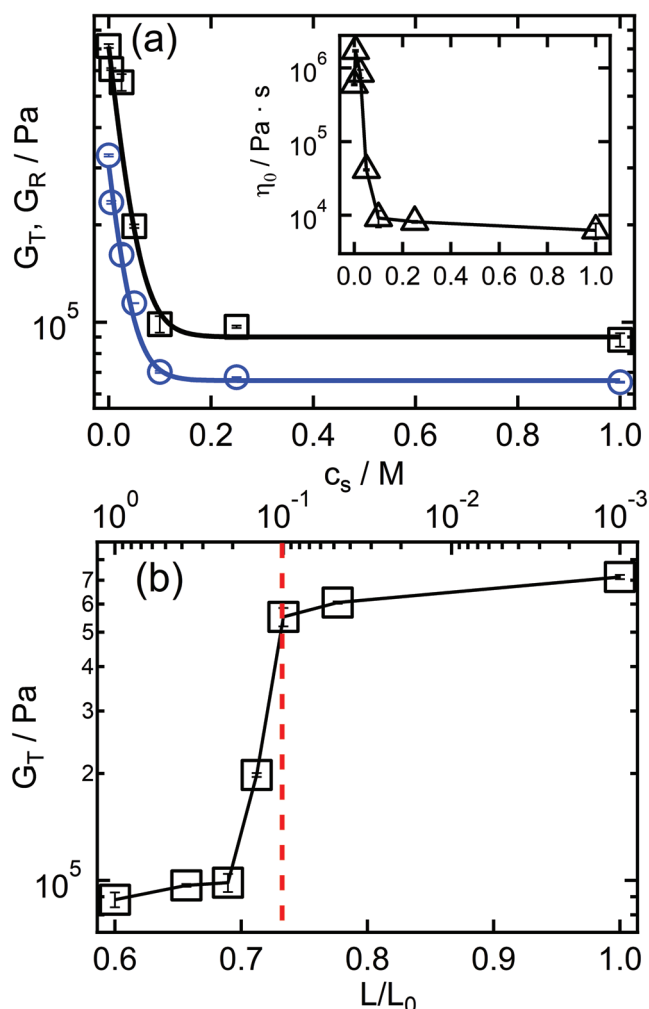


Figure 4. Best-fit parameters as a function of c_s , obtained by modeling the force-relaxation curves of Figure 3 by means of Equation (3). a) Total modulus $G_T = G_0 + G_R$ (\square) and residual modulus G_R (\circ). The lines are the best fits of the data of the following expression: $G_i = G_i^0 \exp(-c_s/c_s^0) + B$, with $i = T, R$. Inset: the viscosity η_0 , same x-axis as in the main plot. b) G_T as a function of relative corona thickness L/L_0 . The top axis reports the corresponding salt concentration c_s . Error bars correspond to one standard deviation obtained from the fits.

$\langle \tau \rangle$ (Figure 5), which suggests that while the static stiffness of the particles decreases monotonically with increasing the salt concentration, the dynamic response of these colloidal systems is more complex; hence the need of measuring the frequency-dependent viscoelastic moduli for a better understanding of their dynamics, as described below.

2.3. Indentation and Relaxation Experiments: Frequency-Dependent Viscoelastic Moduli

An alternative approach to determine the viscoelastic properties of the colloidal particles is via the Fourier transform of the time-dependent force relaxation measurement $F(t)$. This is possible because the material's complex shear modulus $G^*(\omega) = G'(\omega) + iG''(\omega)$ is defined as the Fourier transform of the time derivative of $G(t)$ and therefore by considering Equation (2) one obtains

$$G^*(\omega) = i\omega \hat{G}(\omega) = i\omega C \hat{F}(\omega) = G'(\omega) + iG''(\omega) \quad (4)$$

$$C = \frac{3(1-\nu)}{8\delta_0^{3/2}} \left[\left(\frac{1}{R^*} \right)^{1/3} + \left(\frac{1}{R_2} \right)^{1/3} \right]^{3/2} \quad (5)$$

where $G'(\omega)$ and $G''(\omega)$ are the materials' viscoelastic moduli describing the frequency-dependent elastic and viscous character of the system, respectively. The Fourier transform is performed by using the analytical method proposed by Evans and Tassieri.^[25,49,50] Before performing the Fourier transform, the force-relaxation curves were smoothed using a Savitzky-Goyal filter to reduce the disruptive contribution of the noises, given the integral nature of the Fourier transform. Notice that the use of such a filter does not alter the shape of the relaxation curves. An advantage of the direct Fourier transform of the experimental data relies on the absence of any preconceived model for describing the viscoelastic behavior of the material. A similar approach has been successfully applied in different studies^[50,51] and recently adopted for the evaluation of the viscoelastic properties of single cells, after testing the effectiveness of the analytical procedure on different complex soft materials.^[25]

Figure 6 shows the frequency-dependent viscoelastic moduli of the colloidal particles dispersed in water at different salt concentrations. The storage modulus $G'(\omega)$ shows a reduction with the increase of c_s , mirroring the reduction of the stiffness deduced from the best fits of $G(t)$ described in the previous section. This can be further corroborated by extracting the high-frequency value of the storage modulus, G'_h as a function of c_s as shown in Figure 7a. The dependence of G'_h on c_s can be described by means of an exponential decay, $G'_h \propto A + B \exp[-(c_s/c_s^0)]$ with $c_s^0 \approx 0.026$ M, in close agreement with the results obtained from the analysis of G_T and G_R , and therefore educing the same conclusions.

The frequency dependence of the moduli and their relative variation provide additional crucial information on the viscoelastic nature of the colloidal particles. Indeed, the DNA corona is a dense polyelectrolyte solution, which is intrinsically viscoelastic. In particular, while the storage modulus $G'(\omega)$

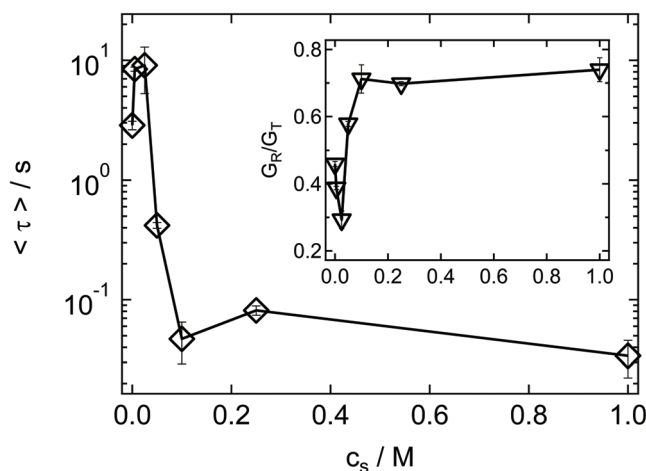


Figure 5. Mean relaxation time $\langle \tau \rangle = \eta_0/G_0$. Inset: ratio between the residual and the total modulus, G_R/G_T , same x-axis as in the main plot. Error bars for $\langle \tau \rangle$ and G_R/G_T were obtained from standard error propagation using the uncertainties of η_0 , G_0 , G_R , and G_T .

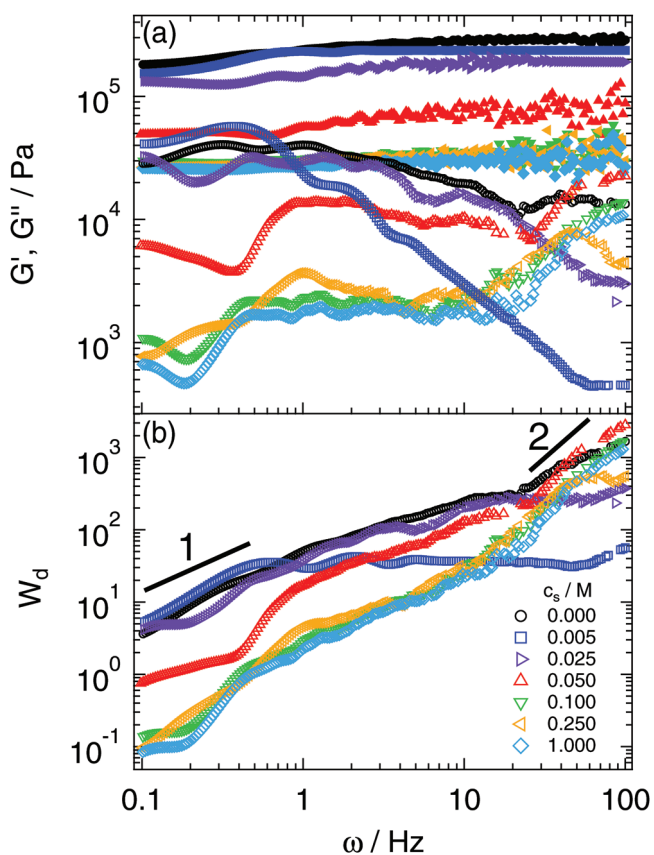


Figure 6. a) Frequency behavior of the storage $G'(\omega)$ (solid symbols) and the loss $G''(\omega)$ (open symbols) moduli and b) of the average energy dissipated in a cycle, W_d , obtained from indentation and relaxation experiments for different salt concentrations, as indicated in the legend. Lines in (b) are guides for power laws with exponents 1 and 2. Frequency-dependent viscoelastic moduli in (a) were obtained by Fourier transforming $G(t)$ data in Figure 3a according to Equations (4) and (5).

shows a weak frequency dependence for all the explored salt concentrations, indicating a solid-like behavior, $G''(\omega)$ in the absence of salt shows an almost constant value up to a maximum frequency of $\omega \approx 1.5$ Hz, after which the loss modulus starts to decrease. This indicates a maximum of energy dissipation that can be associated with dsDNA chains' structural relaxation. Moreover, it is interesting to notice that the region of maximum dissipation shifts to slightly lower frequencies for $c_s = 0.005$ M, and then it moves back to almost the same value obtained in the salt-free solution at $c_s = 0.025$ M. At relatively larger values of c_s , the $G''(\omega)$ maximum shifts toward the higher end of the explored frequencies, implying a substantial acceleration of the relaxation processes occurring at relatively small length scales. To quantify these changes we plot in the inset of Figure 7a the inverse of the frequency at which the maximum of $G''(\omega)$ is observed; i.e., a characteristic relaxation time τ_{max} of the topological changes of the dsDNA chains as a function of c_s . Notably, as we might have already anticipated, not only both the terms of G'_h and τ_{max} show the same behavior of G_T (or G_R) and $\langle \tau \rangle$, respectively, but also they show very similar values. Therefore, we could speculate that the two analytical approaches are qualitatively and quantitatively congruent. Nonetheless,

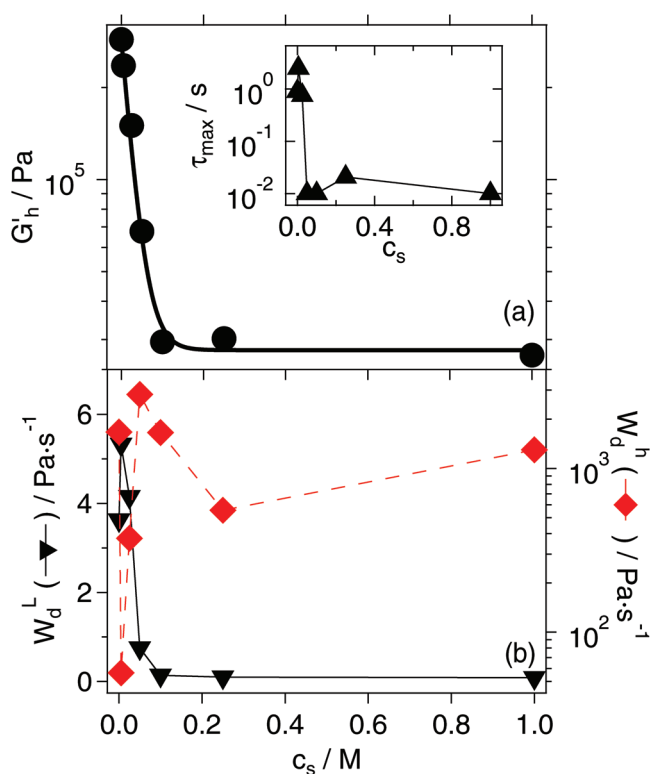


Figure 7. a) High frequency storage modulus G'_h as a function of salt concentration c_s . The solid line represents a fit to an exponential decay. Inset: time τ_{max} at which the maximum of G'' is observed, as a function of c_s . b) Value of the energy dissipated in a cycle, W_d , calculated for the lowest (W_d^L , left axis) and highest (W_d^h , right axis) frequencies, as a function of c_s .

the direct Fourier transform of the force–relaxation curve, as already stressed, does not need the assumption of any preconceived model describing the viscoelastic nature of the system under investigation.

Additional information can be obtained by calculating the average energy dissipated within a cycle at a specific frequency^[52]: $W_d(\omega) = (1/2)\omega G''(\omega)\delta_0^2$ (see Figure 6b). At $c_s = 0$ and at relatively low frequencies (i.e., below 1 Hz), we observe an almost linear proportionality of $W_d(\omega)$ with ω ; whereas, at higher frequencies the slope is smaller than 1, indicating a reduction of dissipation and a more pronounced solid-like behavior. At a salt concentration of $c_s = 0.005$ M, a similar behavior is observed at relatively low frequencies, but a pronounced change of the slope of $W_d(\omega)$ is observed at a frequency value of $\omega = 0.5$ Hz; then the gradient remains approximately equal to zero, indicating a solid-like behavior of the colloidal particle. At a salt concentration of $c_s = 0.025$ M the colloids show a similar behavior to those in salt-free solution up to a frequency value of circa $\omega = 20$ Hz, then they also show a solid-like behavior. At salt concentrations of $c_s = 0.05$ M and higher, the dissipated energy shows again a marked change in the frequency dependence. The dissipation increases initially almost quadratically with frequency (this is clearer for $c_s = 0.1$ M and higher), then at intermediate frequencies it is almost linearly proportional to ω up to circa $\omega \approx 20$ Hz, after which it increases again quadratically, $W_d(\omega) \propto \omega^2$. In order to

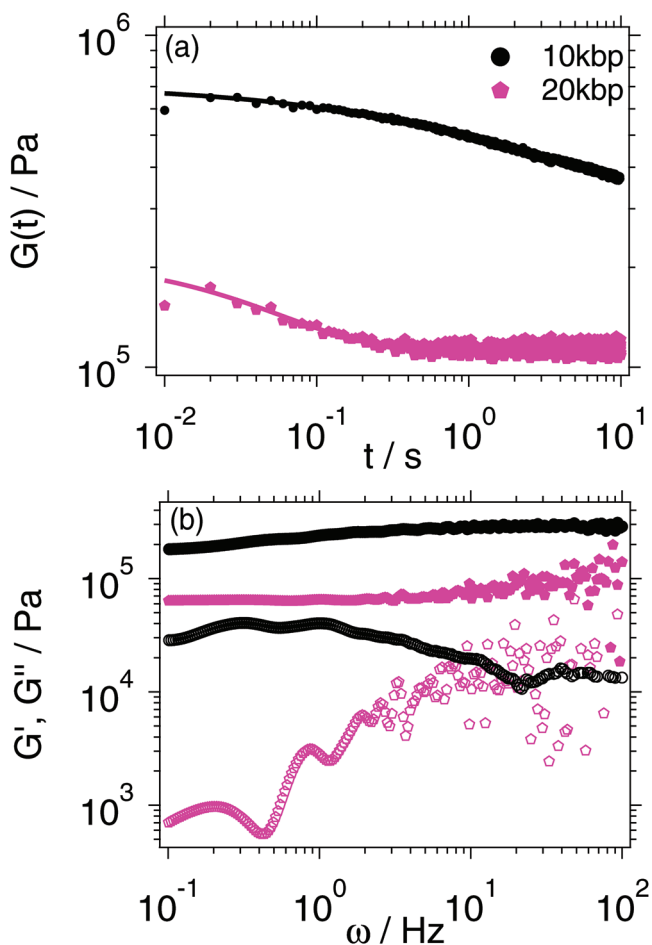


Figure 8. a) Time-dependent shear relaxation modulus and b) frequency-dependent viscoelastic moduli, $G'(\omega)$ (solid symbols) and $G''(\omega)$ (open symbols), obtained from indentation and relaxation experiments on PS particles decorated with 10 kbp (circles) or 20 kbp (pentagons) dsDNA chains. Frequency-dependent viscoelastic moduli in (b) were obtained by Fourier transforming $G(t)$ data in (a) according to Equations (4) and (5).

better elucidate these results, the values of the energy dissipation determined at the extremes of the explored frequencies (i.e., W_d^l at a frequency of $\omega = 0.1$ Hz and W_d^h at a frequency $\omega = 100$ Hz) are reported in Figure 7b. From the latter, one can observe that there is a moderate increase of W_d^l from a salt-free condition to $c_s = 0.005$ M, followed by a monotonic decrease for higher values of c_s . This behavior closely resembles those of the relaxation times $\langle \tau \rangle$ and τ_{\max} . On the other hand, the behavior of W_d^h is more complex, showing an initial decrease with a relative minimum value at $c_s = 0.005$ M, followed by a relative maximum at $c_s = 0.05$ M and further smaller variations at larger values of c_s . The similarities between W_d^l , $\langle \tau \rangle$ and τ_{\max} induce us to infer that small dissipation values are associated with the topological changes of the corona, possibly related to the change in stiffness of the single DNA chains (i.e., from rod-like to coil-like, as c_s increases). At high frequencies, W_d^h indicates that the energy is dissipated more efficiently by the samples with a collapsed corona and showing lower values of G_T . Here we speculate that this phenomena might be governed by the single DNA chain relaxation, which is faster for flexible (screened) chains at

high salt concentrations than for rigid (charged) chains at small salt concentration.

2.4. Effect of dsDNA Chain Length on Viscoelasticity

To test the influence of the length of the dsDNA chains on the viscoelastic behavior of the colloidal particles, we performed indentation and relaxation experiments on particles with longer grafted DNA chains (i.e., 20 kbp long) and in salt-free solution. Both the colloids had the same grafting density (200 000 chains) and size of the PS core ($R_{PS} = 0.49 \mu\text{m}$). We observed that the magnitude of the modulus $G(t)$ of the colloidal particles covered with 10 kbp chains is about three times bigger than the particles covered with 20 kbp chains (Figure 8a), and with a longer relaxation process. Indeed, by fitting the experimental data of the 20 kbp system with Equation (3) we obtain $G_R \approx 1.1 \times 10^5 \pm 0.03$ Pa, $G_T \approx 2.1 \times 10^5 \pm 0.05$ Pa, and $\tau \approx 0.04 \pm 0.005$ s. The first two values are comparable to those obtained for the smaller colloidal particles in a 0.05 M NaCl solution, whereas the value of τ is closer and even slightly smaller than those obtained for $c_s \geq 0.1$ M. This suggests that a longer chain length induces changes similar to the addition of salt, however, with a different balance between the viscous and elastic contribution to the final mechanical properties of the colloid. Figure 8b shows the viscoelastic moduli obtained by Fourier transforming the time-dependent shear relaxation modulus. The storage modulus decreases in magnitude while keeping a similar frequency behavior, whereas the loss modulus shows the qualitative change discussed in the previous section for the largest values of c_s , i.e., the maximum moves to larger frequencies indicating a faster relaxation of the system. We can therefore conclude that a thicker corona also leads to a significant softening of the particles.

2.5. Discussion

The reduction of the particle stiffness with increasing of the amount of salt in solution can be interpreted in terms of the morphological variations of the dsDNA corona, which mimics in general those of brushes formed by long polyelectrolyte chains. At very low salt concentration the corona absorbs almost all counterions and the chains are completely stretched in order to maximize the available volume for the mobile counterions. With addition of salt the osmotic imbalance between the inside of the corona and the bulk is progressively removed and the chains become more flexible, thus their configuration becomes increasingly random reducing the effective size of the corona, until they collapse at large salt concentrations. The softening of the particles shows a pronounced exponential dependence on salt concentration and an abrupt transition at a critical corona size $L_s \approx 0.72 L_0$, which are dictated by the changes in the counterion distribution. It should be noticed that the observed softening of the dsDNA corona is much more pronounced than the increased flexibility of isolated dsDNA chains with increasing salt concentration, which has been determined by existing studies on the persistence length (or equivalently the Young's modulus) of single dsDNA chains.^[53–55] Indeed, in the

latter studies the dependence of E on c_s is milder; i.e., roughly inversely proportional to c_s . This is indicative that the entropic effects of the counterions in a dense dsDNA brush are dominating its mechanical properties.

The reduction of stiffness with increasing c_s is consistent with recent model systems used to calculate the elastic properties of dense films of shorter (few tenths of nm) dsDNA chains on a substrate as a function of salt concentration.^[56,57] These models are static, i.e., they only predict the elasticity of the films via its Young's modulus (E). These films are typically used as coatings for AFM microcantilevers for biodetection.^[58] In particular, Wu and co-workers^[56] have presented a bead-chain model where the DNA chain is divided into spherical fragments connected by elastic rods, which interact with the fragments of other chains through a Yukawa potential. By solving numerically the model, Wu and co-workers obtained the values of the Young's modulus as a function of salt concentration, which is in good agreement with our findings and shows an exponential decay similar to those found in this work for G'_h , G'_T or G'_R . In particular, the data of Wu and co-workers^[56] for the Young's modulus can be described through the relation: $E \approx A + B \exp[-(c_s/c_s^0)]$ (see the Supporting Information), with $c_s^0 \approx 0.01$ M in their case. Such behavior of the Young's modulus as function of c_s has been explained by Wu and co-workers^[56] in terms of increased flexibility of the dsDNA chain together with the contribution of the complex interactions between different dsDNA chains in the brush. We show here that the counterion distribution governing the configurations of the dsDNA chains in the corona is the dominant contribution to the softening. The growth of DNA flexibility with increasing c_s is consistent with the faster relaxation process of the force and the increase of the frequency at which the maximum of G'' is observed. Indeed, the dynamics of the semi-flexible dsDNA chains are expected to become faster with decreasing their persistence length.^[59,60] At the same time, the non-monotonic behavior of the ratio of the viscous to the elastic moduli as a function of salt concentration cannot be directly related to any existing prediction and will need further investigation.

Finally, it must be noted that the decrease of the particle stiffness with the increase of chain length should not be attributed to variations of the dsDNA flexibility. This is because in the low-salt limit the persistence length of sufficiently long dsDNA does not depend on the chain length.^[61] We could speculate that the reduced elasticity of the colloidal particles having longer chain lengths is related to a lower DNA density at the external surface of the corona for longer chains than shorter ones.

3. Conclusions

Using AFM indentation and relaxation experiments, we determined the viscoelastic properties of single-particle hairy dsDNA colloids in suspension as a function of the ionic strength and the dsDNA chain length. By adopting two different analytical approaches, i.e., via either i) modeling the force relaxation curves by using a modified Maxwell model or ii) a direct Fourier transform of the shear relaxation modulus to obtain the frequency-dependent moduli, we consistently show a pronounced reduction of the colloidal stiffness by increasing the ionic

strength of the solution. This occurs exponentially as a function of the salt concentration, with a sharp decrease at $c_s \lesssim 0.026$ M, which in terms of the brush size corresponds to a critical size of $L_s \approx 0.72 L_0$. The stiffness reduction of the colloids as function of the salt concentration is also manifested with a faster relaxation of the force, which relates to a shift of the maximum of $G''(\omega)$ (i.e., the point of maximum dissipation) to a higher frequency value. We interpret these results as the manifestation of the changes in the counterion distribution in the polyelectrolyte brush with increasing ionic strength, which strongly affect the chain conformations and chain-chain interactions. Indeed, the moduli of the dsDNA brush show a much stronger dependence on salt concentration than the stiffness of isolated dsDNA chains.^[53–55] Our results are in agreement with recent numerical studies on films of shorter dsDNA chains grafted on substrates.^[56,57] A closer look at the frequency-dependent viscoelastic properties suggests that the energy dissipation at low frequencies (i.e., long times) is dominated by the collective force relaxation in the corona, whereas at high frequencies (i.e., short times) chain dynamics might be more important. Finally, we report that particles with a thicker DNA corona are softer, which can be associated with a lower DNA density in the outer side of the corona and/or a weaker contribution of the rigid core of the colloid.

To conclude, we would like to highlight that both the results and the method presented in this work open the way to a systematic investigation of the viscoelastic properties of colloidal particles of different nature, including microgel particles, soft composite particles, micelles, and others. These properties are of great importance for the understanding of the phase behavior of these systems. In particular, we stress that the viscoelastic properties of colloidal particles can be determined through a model-free method, based on the Fourier transform of force relaxation curves.

4. Experimental Section

Synthesis of DNA Star Polyelectrolyte Colloids and Dispersions' Preparation: The procedure to obtain DNA star polyelectrolyte colloids was described in detail before.^[32] Here, the main steps of the procedure are recalled that can be summarized as follows: i) Double-stranded DNA synthesis through the amplification to 20Kbp and 10Kbp end-biotinylated fragments via Polymerase Chain Reaction (PCR). ii) Grafting of DNA chains to the streptavidin functionalized surface of polystyrene beads ($R_{ps} = 0.49$ μm). The particles are then dispersed in deionized water and different saline buffer solutions containing 5×10^{-3} , 2.5×10^{-2} , 5×10^{-2} , 10^{-1} , 2.5×10^{-1} , and 1 M of NaCl. For a fraction of the particles, the DNA was prelabeled with YOYO-1 (Thermofisher) at a dye—DNA base pair ratio of 1:25 and the colloids were characterized by confocal microscopy revealing a particle size $R \approx 8$ μm in pure water solution. Dispersions with a particle volume fraction $\phi = 0.01$ were prepared for the experiments.

Sample Preparation for AFM Measurements: A drop of dispersion was deposited onto an untreated borosilicate glass microscope slide. Due to the van der Waals interactions between double-stranded DNA and borosilicate glass, particles stuck to the glass surface.^[62] These interactions were of short-range action,^[62] but strong enough to hold the colloids firmly in place on the glass surface. Moreover, since they only extended over nanometer length scales, they would not affect the chains configuration on the side subjected to the AFM indentation. The dispersion was sufficiently dilute such that isolated particles could

be easily found, as shown in Figure S1 (Supporting Information). The duration of a typical experiment was a few minutes, which guaranteed that no significant water evaporation occurred over this time interval.

AFM Measurements: Indentation and relaxation experiments were performed using an Alpha 300a AFM (WiTec). Colloidal Probe tips (SQube) where an 8 μm (diameter) polystyrene bead was glued to a cantilever with a nominal force constant $C = 42 \text{ N m}^{-1}$ and length $L = 125 \mu\text{m}$ were used for all the measurements. The spring constant of the cantilever was independently determined using the Off-end loading method^[63] and compared well with the force constant obtained from the provider. The AFM tip was immersed in the droplet for the measurement.

Supporting Information

Supporting Information is available from the Wiley Online Library or from the author.

Acknowledgements

M.L., J.A.M.G., I.C.R.S., and A.M.B. acknowledge support from the Consejo Nacional de Ciencias y Tecnologia (CONACYT, Mexico) through grants Nos. FC-2015-2/1155, LANIMFE-279887-2017, and CB-2015-01-257636. M.T. acknowledges support via EPSRC grant (EP/R035067/1, EP/R035563/1, and EP/R035156/1). The authors thank A. Zaccone, E. Zaccarelli, and S. Sennato for insightful discussions.

Conflict of Interest

The authors declare no conflict of interest.

Keywords

AFM, brush, colloids, dsDNA, polyelectrolytes, viscoelasticity

Received: August 28, 2019
Published online: August 28, 2019

- [1] R. Larson, *The Structure and Rheology of Complex Fluids*, Oxford University Press, New York **1999**.
- [2] J. Mewis, N. J. Wagner, *Colloidal Suspension Rheology*, Cambridge University Press, New York **2012**.
- [3] W. B. Russel, D. A. Saville, W. R. Schowalter, *Colloidal Dispersions*, Cambridge Monographs on Mechanics, Cambridge University Press, **1989**.
- [4] S. Ravaine, E. Duguet, *Curr. Opin. Colloid Interface Sci.* **2017**, *30*, 45.
- [5] L. A. Lyon, A. Fernandez-Nieves, *Annu. Rev. Phys. Chem.* **2012**, *63*, 25.
- [6] D. Vlassopoulos, M. Cloitre, *Curr. Opin. Colloid Interface Sci.* **2014**, *19*, 561.
- [7] C. N. Likos, H. Löwen, M. Watzlawek, B. Abbas, O. Jucknischke, J. Allgaier, D. Richter, *Phys. Rev. Lett.* **1998**, *80*, 4450.
- [8] S. A. Kim, K.-J. Jeong, A. Yethiraj, M. K. Mahanthappa, *Proc. Natl. Acad. Sci. USA* **2017**, *114*, 4072.
- [9] L. Athanasopoulou, P. Zihlerl, *Soft Matter* **2017**, *13*, 1463.
- [10] A.-K. Doukas, C. N. Likos, P. Zihlerl, *Soft Matter* **2018**, *14*, 3063.
- [11] M. Pelaez-Fernandez, A. Souslov, L. A. Lyon, P. M. Goldbart, A. Fernandez-Nieves, *Phys. Rev. Lett.* **2015**, *114*, 098303.
- [12] A. Scotti, U. Gasser, E. S. Herman, M. Pelaez-Fernandez, J. Han, A. Menzel, L. A. Lyon, A. Fernández-Nieves, *Proc. Natl. Acad. Sci. USA* **2016**, *113*, 5576.
- [13] K. N. Nordstrom, E. Verneuil, W. G. Ellenbroek, T. C. Lubensky, J. P. Gollub, D. J. Durian, *Phys. Rev. E* **2010**, *82*, 041403.
- [14] H. M. Phillips, M. S. Steinberg, *Proc. Natl. Acad. Sci. USA* **1969**, *64*, 121.
- [15] K. Guevorkian, M.-J. Colbert, M. Durth, S. Dufour, F. Brochard-Wyart, *Phys. Rev. Lett.* **2010**, *104*, 218101.
- [16] H. M. Wyss, T. Franke, E. Mele, D. A. Weitz, *Soft Matter* **2010**, *6*, 4550.
- [17] B. Sierra-Martin, J. Frederick, Y. Laporte, *Colloid Polym. Sci.* **2011**, *289*, 721.
- [18] A. R. Abate, L. Han, L. Jin, Z. Suo, D. A. Weitz, *Soft Matter* **2012**, *8*, 10032.
- [19] C.-H. Lin, C.-K. Wang, Y.-A. Chen, C.-C. Peng, W.-H. Liao, Y.-C. Tung, *Sci. Rep.* **2016**, *6*, 36425.
- [20] S. Biggs, G. Spinks, *J. Adhes. Sci. Technol.* **1998**, *12*, 461.
- [21] S. M. Hashmi, E. R. Dufresne, *Soft Matter* **2009**, *5*, 3682.
- [22] D. Guo, J. Li, G. Xie, Y. Wang, J. Luo, *Langmuir* **2014**, *30*, 7206.
- [23] G. Forgacs, R. A. Foty, Y. Shafir, M. S. Steinberg, *Biophys. J.* **1998**, *74*, 2227.
- [24] E. M. Darling, S. Zauscher, J. A. Block, F. Guilak, *Biophys. J.* **2007**, *92*, 1784.
- [25] Y. H. Chim, L. M. Mason, N. Rath, M. F. Olson, M. Tassieri, H. Yin, *Sci. Rep.* **2018**, *8*, 14462.
- [26] B. Carmichael, H. Babahosseini, S. N. Mahmoodi, M. Agah, *Phys. Biol.* **2015**, *12*, 046001.
- [27] J. Alcaraz, L. Buscemi, M. Grabulosa, X. Trepas, B. Fabry, R. Farré, D. Navajas, *Biophys. J.* **2003**, *84*, 2071.
- [28] Y.-B. Lu, K. Franze, G. Seifert, C. Steinhäuser, F. Kirchhoff, H. Wolburg, J. Guck, P. Janmey, E.-Q. Wei, J. Käs, A. Reichenbach, *Proc. Natl. Acad. Sci. USA* **2006**, *103*, 17759.
- [29] A. X. Cartagena-Rivera, W.-H. Wang, R. L. Geahlen, A. Raman, *Sci. Rep.* **2015**, *5*, 11692.
- [30] H. T. Nia, I. S. Bozchalooi, Y. Li, L. Han, H.-H. Hung, E. Frank, K. Youcef-Toumi, C. Ortiz, A. Grodzinsky, *Biophys. J.* **2013**, *104*, 1529.
- [31] A. Rigato, A. Miyagi, S. Scheuring, F. Rico, *Nat. Phys.* **2017**, *13*, 771.
- [32] J. Zhang, P. M. Lettinga, J. K. G. Dhont, E. Stiakakis, *Phys. Rev. Lett.* **2014**, *113*, 268303.
- [33] R. Hariharan, C. Biver, J. Mays, W. B. Russel, *Macromolecules* **1998**, *31*, 7506.
- [34] G. M. Conley, P. Aebischer, S. Nöjd, P. Schurtenberger, F. Scheffold, *Sci. Adv.* **2017**, *3*, 1700969.
- [35] A. Jusufi, C. N. Likos, *Rev. Mod. Phys.* **2009**, *81*, 1753.
- [36] X. Chen, R. P. Richter, *Interface Focus* **2019**, *9*, 20180061.
- [37] E. S. Dehghani, S. N. Ramakrishna, N. D. Spencer, E. M. Benetti, *Macromolecules* **2017**, *50*, 2932.
- [38] S. Attili, R. P. Richter, *Langmuir* **2012**, *28*, 3206.
- [39] X. Sui, S. Zapotoczny, E. M. Benetti, P. Schön, G. J. Vancso, *J. Mater. Chem.* **2010**, *20*, 4981.
- [40] O. Azzaroni, S. Moya, T. Farhan, A. A. Brown, W. T. S. Huck, *Macromolecules* **2005**, *38*, 10192.
- [41] H. Hertz, J. Reine, *Angew. Math.* **1882**, *92*, 156.
- [42] D. C. Lin, E. K. Dimitriadis, F. Horkay, *J. Biomech. Eng.* **2006**, *129*, 430.
- [43] M. Radmacher, M. Fritz, C. Kacher, J. Cleveland, P. Hansma, *Biophys. J.* **1996**, *70*, 556.
- [44] E. H. Lee, J. R. M. Radok, *J. Appl. Mech.* **1960**, *27*, 438.
- [45] Z. Zhou, H. Lu, *Mech. Time-Depend. Mater.* **2010**, *14*, 1.
- [46] E. K. Dimitriadis, F. Horkay, J. Maresca, B. Kachar, R. S. Chadwick, *Biophys. J.* **2002**, *82*, 2798.
- [47] J. Gore, Z. Bryant, M. Nöllmann, M. U. Le, N. R. Cozzarelli, C. Bustamante, *Nature* **2006**, *442*, 836.
- [48] C. W. Macosko, R. G. Larson, *Rheology: Principles, Measurements, and Applications*, VCH, New York, NY **1994**, pp xviii, 550 p.
- [49] R. M. L. Evans, M. Tassieri, D. Auhl, T. A. Waigh, *Phys. Rev. E* **2009**, *80*, 012501.

- [50] M. Tassieri, M. Laurati, D. J. Curtis, D. W. Auhl, S. Coppola, A. Scalfati, K. Hawkins, P. R. Williams, J. M. Cooper, *J. Rheol.* **2016**, *60*, 649.
- [51] M. Tassieri, J. Ramírez, N. C. Karayiannis, S. K. Sukumaran, Y. Masubuchi, *Macromolecules* **2018**, *51*, 5055.
- [52] D. Chandler, *Introduction to Modern Statistical Mechanics*, Oxford University Press, New York **1987**, p 288.
- [53] C. G. Baumann, S. B. Smith, V. A. Bloomfield, C. Bustamante, *Proc. Natl. Acad. Sci.* **1997**, *94*, 6185.
- [54] J. R. Wenner, M. C. Williams, I. Rouzina, V. A. Bloomfield, *Biophys. J.* **2002**, *82*, 3160.
- [55] E. Herrero-Galán, M. E. Fuentes-Perez, C. Carrasco, J. M. Valpuesta, J. L. Carrascosa, F. Moreno-Herrero, J. R. Arias-Gonzalez, *J. Am. Chem. Soc.* **2013**, *135*, 122.
- [56] J.-Z. Wu, W.-L. Meng, H.-S. Tang, N.-H. Zhang, *J. Phys. D: Appl. Phys.* **2017**, *50*, 205401.
- [57] H.-S. Tang, W.-L. Meng, N.-H. Zhang, *Acta Mech. Sin.* **2014**, *30*, 15.
- [58] N.-H. Zhang, J.-Z. Chen, *J. Biomech.* **2009**, *42*, 1483.
- [59] A. Nikoubashman, A. Milchev, K. Binder, *J. Chem. Phys.* **2016**, *145*, 234903.
- [60] M. Tassieri, *Macromol.* **2017**, *50*, 5611.
- [61] A. Naji, C. Seidel, R. R. Netz, in *Surface-Initiated Polymerization II* (Ed: R. Jordan), Springer, Berlin **2006**, pp. 149.
- [62] B. Shi, Y. K. Shin, A. A. Hassanali, S. J. Singer, *J. Phys. Chem. B* **2015**, *119*, 11030.
- [63] C. T. Gibson, G. S. Watson, S. Myhra, *Scanning* **1997**, *19*, 564.